PAPER • OPEN ACCESS

Actuator grid method for turbulence generation applied to yawed wind turbines

To cite this article: F. Houtin–Mongrolle *et al* 2020 *J. Phys.: Conf. Ser.* **1618** 062064

View the article online for updates and enhancements.

Actuator grid method for turbulence generation applied to yawed wind turbines

F. Houtin–Mongrolle[1], P. Benard[1], V. Moureau[1], G. Lartigue[1] L. Bricteux[2], J. Reveillon[1]

[1]Normandie Univ, INSA Rouen, UNIROUEN, CNRS, CORIA, Rouen 76000, France
[2]Université de Mons (UMONS), Polytechnic Faculty, Belgium

E-mail: `felix.houtin-mongrolle@coria.fr`

Abstract. The aerodynamics of yawed wind turbine wakes remains a major investigation topic, especially for the use of yaw angle in control strategies. Large-Eddy Simulations are employed here to study the influence of yaw and inflow conditions on the prediction of the wind turbine wake structure. A single wind turbine setup with different yaw angles and three different inflow conditions is investigated and discussed with respect to experimental data. The wind turbine blades are modeled using the actuator line method (ALM) while tower and nacelle are represented with a body-fitted unstructured mesh. The high levels of upstream turbulence, experimentally generated by turbulence grids, are emulated here with oscillating ALM. Such approach demonstrates to be highly predictive on the turbulent flow characteristics compared to the emptied wind tunnel experimental data. Results with turbine show good agreement to the experiment data with only a slight overestimation on the magnitude of the wake deflection due to yaw. When compared to a deflection model, the confinement of the wind tunnel is highlighted. The radial and azimuthal time-averaged angle of attack exhibits a high probability of dynamic stall near the hub for a yawed turbine. These results show large discrepancies on the blade loading, highlighting the need for improved and specific models.

1. Introduction

Maximizing the electric power generated in offshore wind farms is one important energetic and environmental challenge. In these wind farms, individual turbines are subjected to the changing characteristics of the atmospheric boundary layer but they are also exposed to the wakes of other turbines. The wake from an upstream turbine leads to an increase in turbulent intensity and fatigue loading of downstream turbines. New control strategies such as inducing a wind turbine yaw angle seem relevant to reduce wake interactions and associated power losses [1]. However, the yawed turbine aerodynamics is modified and leads to conditions that are out of the validity range of engineering models. Since experimental investigations on actual wind farms are difficult to carry out and given the constant growth of computational resources, high-order numerical simulations tend to be a promising approach [2]. Despite these resources, the limiting factor of numerical simulations remains the high Reynolds number of the flow around the rotor blades. Indeed, the length scales of a fully-resolved wind turbine simulation range from a fraction of the boundary-layer thickness of the rotor blades to the size of the largest eddies in the atmospheric boundary layer. Therewith modeling strategies are necessary.
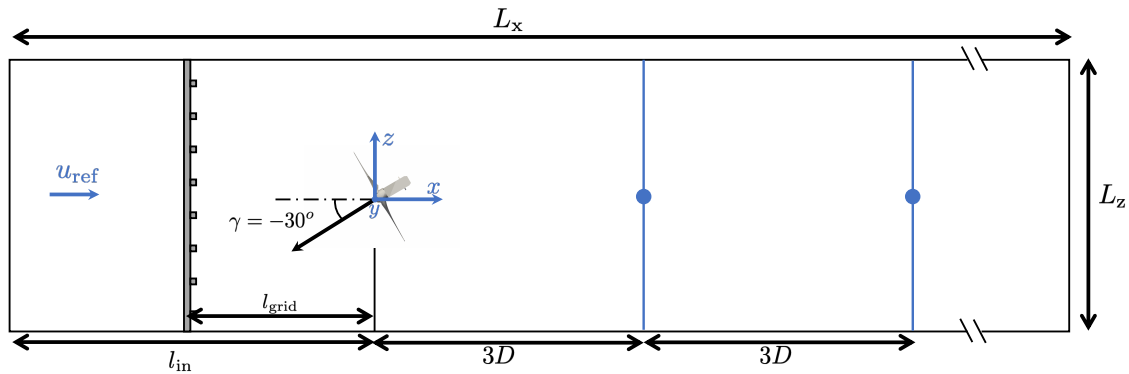
Figure 1. Top view of yawed turbine setup according to the reference coordinate system in the wind tunnel. Blue lines (horizontal profiles) and dot (vertical profiles) at $3D$ and $6D$ indicate where the time-averaged streamwise velocity and streamwise turbulent stress are extracted. The position of the turbulence grids for inflow (ii) and (iii) are represented. The wind tunnel dimensions are $L_x \times L_y \times L_z = 14 \times 1.801 \times 2.71 \, \mathrm{m}^3$.

The present state-of-the-art strategy relies on the actuator line method (ALM). Developped by Sørensen and Shen [3], this approach models each rotor blade as a line force in the same way as the blade element method. It has been widely used with Large-Eddy Simulations (LES) since the constraint is released from the limiting small scales of the flow around the blade geometry. Nevertheless such method suffers from various modeling errors, especially in the computation of the turbine loads. Many corrections [4, 5] of the loads have been tested under optimal conditions but the case of yawed turbines remains an open topic.

This paper studies the wake of a single wind turbine setup for different yaw angles ($+30°$, $0°$ and $-30°$) and the effect of three different inflows: (i) uniform laminar, (ii) uniform turbulent and (iii) non-uniform shear turbulent. The numerical simulations results are compared to the experimental results from J. Bartl et al. [6] operated in the wind tunnel of the Norwegian University of Science and Technology [7].

2. Numerical setup

The incompressible and low-Mach number Navier–Stokes equations are integrated using the YALES2 flow solver [8]. It is a massively-parallel finite-volume solver, which is specifically tailored for Large-Eddy Simulation, and relies on a central 4th-order numerical scheme for spatial discretization, and a 4th-order Runge-Kutta method [9] for the time integration on unstructured grid. Benard et al. [10] have shown the necessity of fairly high order numerics to ensure the proper transport of fine vortical structures present in wind turbine wakes in the context of ALM.

2.1. Wind turbine modeling

In the following, all quantities are non-dimensionalized with the wind turbine diameter $D = 0.894 \, \mathrm{m}$ and the free-stream velocity $u_{\mathrm{ref}} = 10 \, \mathrm{m/s}$. The wind turbine has three operating condition associated to three different yaw angles ($\gamma = +30°$, $0°$ and $-30°$) as depicted in Fig. 1. The blades use the NREL S826 airfoil with variable chord and twist as described in the work of J. Bartl et al. [6]. The rotation speed is imposed to obtain the design tip speed ratio $\lambda_{\mathrm{opt}} = 6$, giving a Reynolds number of approximately $Re_{\mathrm{tip}} \approx 10^5$ at the blade tip. The rotor blades are modeled as actuator lines, i.e. the blade forces are computed at each time step based on the inflow velocity, the angle of attack α and the chord-based Reynolds number lift and drag coefficients $C_{L,D}$ obtained from Satran et al. [7]. After the computation of lift
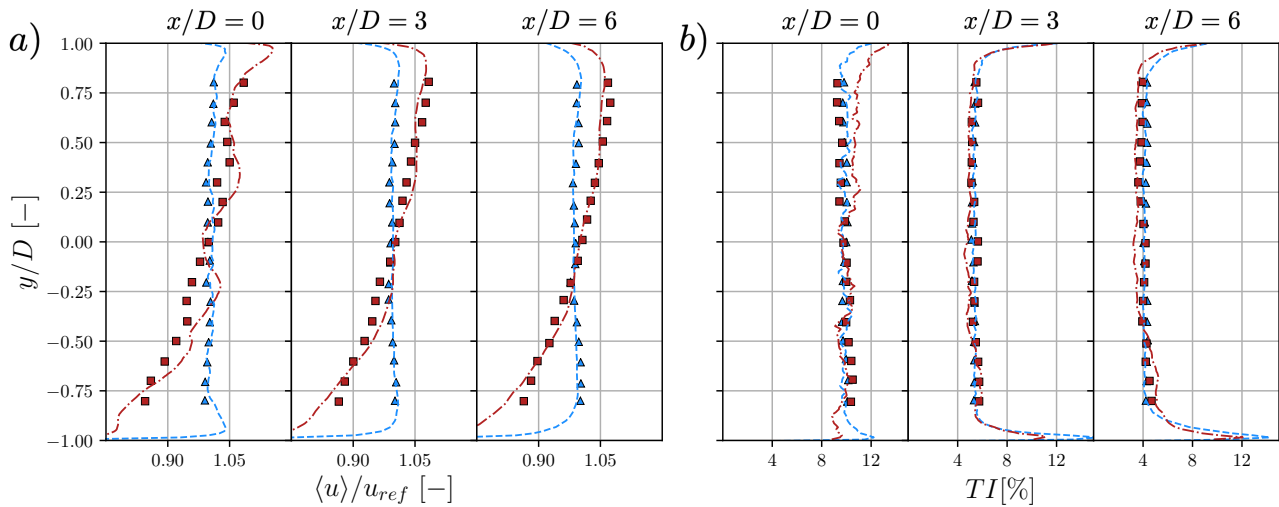
Figure 2. Vertical profiles of the time-averaged a) streamwise velocity and b) the streamwise turbulent intensity in the wind tunnel without the turbine. The results of the inflows generated with the turbulence grids are presented: (ii) Experimental (▲), LES (- - -); (iii) Experimental (■), LES (–·–·)

and drag forces $\mathbf{F}_{2D} = (\mathbf{L}, \mathbf{D})$ at the ALM location using two-dimensional airfoil theory, the blade forces are regularized on the Eulerian grid by performing a convolution using an isotropic three-dimensional Gaussian kernel [3]. In such model, the unsteady force distribution of a blade on the flow is prescribed instead of being resolved by the flow solver. This method is often used with corrections [4, 5] in order to be more predictive on the forces, especially near the tip of the blade. For a yawed turbine, the use of a dynamic stall model is common [11] even if various effects are still undetermined, i.e. the sweep along the blade span impact on the loads. However, in the present work, the authors made the choice to use the ALM without any of these corrections to properly evaluate the error committed here. The tower and nacelle are taken into account by a body-fitted unstructured mesh and the wall model of Duprat et al. [12] is applied on these elements reaching a time-averaged dimensionless wall distance $\langle y^+ \rangle$ around 100 .

2.2. Wind tunnel and turbulence grid
As previously mentioned, three inflows are presented in this study. The turbulent inflows (ii) and (iii) are experimentally generated using static turbulence grids upstream the turbine at $l_{\text{grid}} = 2D$. The numerical domain is constructed to match the wind tunnel dimensions and to be able to emulate the grids effect, setting the inlet distance to the turbine at $l_{\text{in}} = 4D$, see Fig. 1. The wind tunnel walls are taken into account in the same way as the tower and nacelle reaching a $\langle y^+ \rangle$ around 200, which remains in the domain of validity of such model. The specific inflow characteristics are presented in the following:

Inflow (i) exposes the turbine to the free-stream velocity and a low turbulence level ($\text{TI}_{\text{i}} = 0.23\%$) from the wind tunnel, which is far below real atmospheric boundary layer conditions.

The second inflow (ii) is generated using a homogeneous spaced grid of horizontal and vertical square rods. The aim is to expose the turbine to a uniform velocity $u_x = 10\,\text{m/s}$ and a high turbulence intensity $\text{TI}_{\text{ii}} = 10\%$. This level of turbulence is comparable to those of a neutral atmospheric boundary layer, although the inevitable decay of the grid-generated turbulence remains.

The last inflow (iii) is also generated using a turbulence grid but with the horizontal rods

Inflow	Yaw angle γ	# elements	$\Delta t \, [\mu s]$	hCPU [kh]
(ii)	no turbine	157×10^6	357	22
(iii)	no turbine	157×10^6	371	21
(i)	$+30°$	171×10^6	145	29
(ii)	$+30°$	171×10^6	130	46
(iii)	$+30°$	171×10^6	134	43

Table 1. Computational cost associated to the different methods of grid turbulence injection without turbine and for the yaw $+30°$ cases.

clustered closer to the tunnel floor. This grid setup results in exposing the turbine to a non-uniform sheared inflow with a high turbulence level $\text{TI}_{\text{iii}} = 10\%$. The velocity profile and turbulence level gather similar conditions as an onshore site for a neutral atmospheric boundary layer.

The experimental flow measurements from J. Bartl et al. [6] were conducted using a two-component Dantec FiberFlow laser Doppler anemometer system used in differential Doppler mode. More details on the experimental procedure are given in the paper of J. Bartl et al. [6]. In the experimental study, the velocity measurement uncertainties reach up to 5% for the last inflow (iii). Since no other data was available, the experimental uncertainties are not considered.

To take into account the turbulence in the freestream an original strategy based on a dynamic version of the ALM [13] is used. The major aspect of such method is to be able to generate turbulence at a lower degree of empiricism than with precursor methods by using only the geometry of the grid. The grid rods are modeled as the turbine blades but with a fluctuating lift based on the vortex shedding of a square rods. Figure 2 presents the vertical profiles of the streamwise velocity and the turbulence intensity in the empty wind tunnel compared to experimental data [6] for inflow (ii) and iii). Theses results show a very good prediction of both streamwise velocity and turbulence intensity with such modeling approach.

2.3. Computational set-up & performances

In this paper, nine cases are presented on three different grids, and for three yaw conditions. For all cases, the flow-through time τ is taken according to the distance between the grid and $6D$ behind the turbine which results in $\tau = 8D/u_{\text{ref}} = 0.715 \, \text{s}$. The physical duration of the nine simulations is 5τ for the flow establishment and 10τ for statistics accumulation. The computational cost when using high-order numerical simulations must be taken into account. Table 1 gathers the mesh size, the limiting time step and the computational time for the different inflow cases for a yaw angle γ of $+30°$. Theses simulations were performed on 1092 processors each.

It can be noticed here that the major discrepancies in the computational time is due to the inflow condition, with or without turbulence. In addition to that, the wind turbine tower and nacelle add an extra cost due to the small cell size around the turbine geometry. Thus, it requests a larger mesh and induces a lower time step due to the CFL number limitation.

3. Results

3.1. Wake topology

Figure 3 shows the wake vortices development under the first inflow (i) of a single wind turbine at $\gamma = -30°$. The vortices generated at the tip of the blade interact with the tower. The ones generated in the wake of the nacelle interact with the blade-deviated tip vortices at $x = 1D$ and trigger the destabilization of the wake. On the contrary, for the non yawed case, not depicted here, the generated tip vortices will not interact with the wake of the nacelle and the
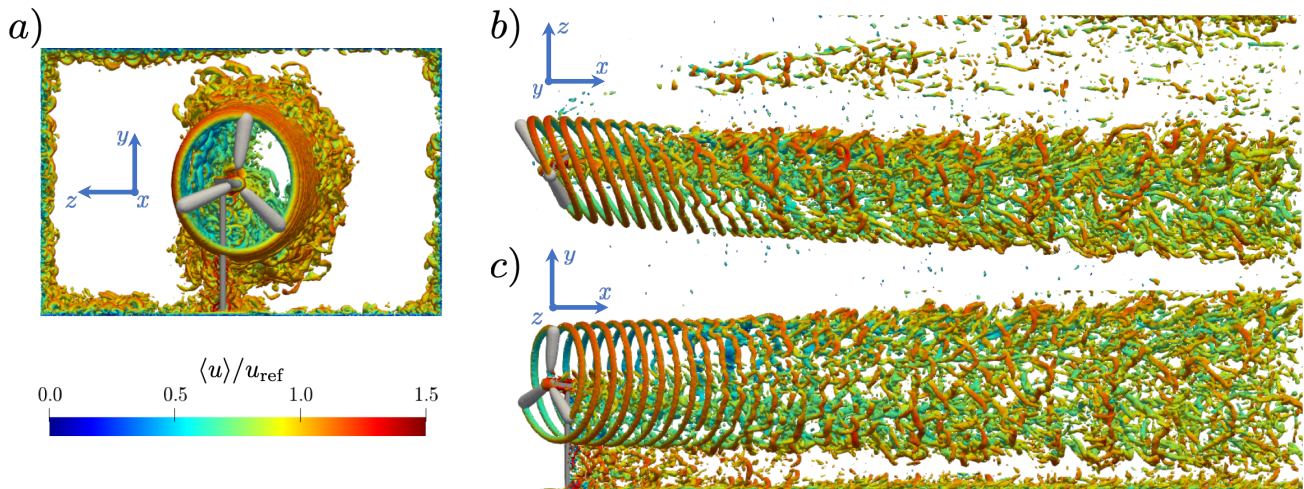
Figure 3. Front a), upper b) and side c) views of the instantaneous 3D visualization of the wake generated by the turbine blades, tower and nacelle at $\gamma = -30°$ under inflow (i) using an iso-contour of the Q criterion colored by flow velocity. The grey iso-surface represents a contour of the volume force applied to the flow by the blades. The tower and nacelle surfaces are in dark grey.

destabilization is delayed to $x = 1.75D$. In Fig. 3 a) and b), one can notice the asymmetry of the bottom turbulent boundary layer in the wind tunnel along z-axis. The simulation for $\gamma = -30°$ is not depicted here but the same effect can be observed on the other side of the tower. For the case without yaw, this asymmetry is not observed. Nevertheless, this effect seems to be due to the confinement of the configuration and not to the yaw angle of the turbine.

Two different inflows (i) and (iii) can be observed through a slice of the instantaneous velocity field in Fig. 4. In Fig. 4 b) with inflow iii), the contour of the volume force in black represents the turbulence grid emulated with the dynamic actuator line method. The wake of the grid rods can be observed at a short distance from the grid and interacts with each other to generate a high level of free-stream turbulence. The rod spacing generates higher velocities on the left and right sides of the tunnel. The wake of the nacelle produces a peak of velocity on the downwind side of the nacelle.

3.2. Inflow and yaw impact on wake

The flow statistics are compared considering the profiles of mean streamwise velocity, Fig. 5 a-c), and streamwise turbulent kinetic energy (TKE), Fig. 5 d-f), at two positions downstream of the turbine for inflow (iii) and for all yaw angle conditions. The velocity deficit is well predicted with respect to experimental data as it can be seen on b) for the non yawed wind turbine. For the yawed cases a) and c), the wake velocity deficit seems to recover faster than in the experimental configuration. Indeed, the velocity deficit tendency remains close to the experiment but is slightly underestimated. The analysis on the TKE is equivalent, the decay of turbulence in the turbine wake being overestimated. The TKE of the non yawed cases presents similar results between LES and experiment. Yet, at $x/D = 3$ simulations present a higher turbulence level in the wake of the nacelle and a lower level at $z/D = -0.25$. No TKE steep profile is present at the nacelle position for the yawed turbines. As observed in subsection 3.1 this seems to be due to the interactions of the tower wake with the tip vortices, mixing and diffusing the TKE. It is important to notice that the level of TKE outside of the wake center is
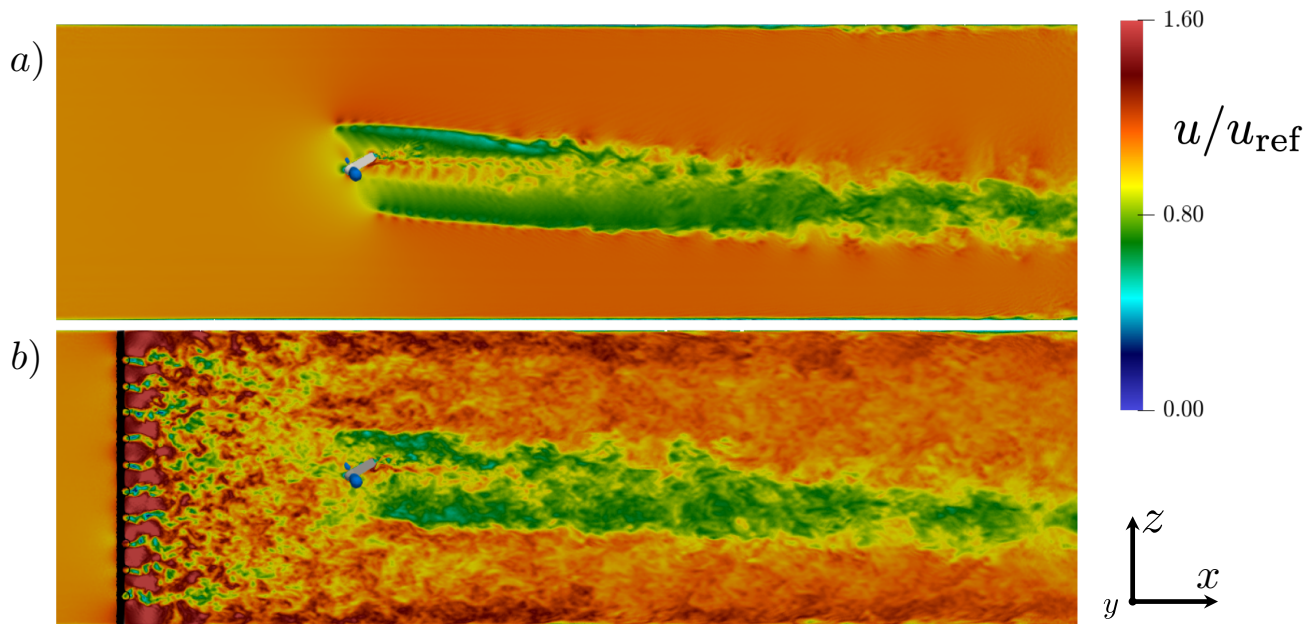
Figure 4. Horizontal slice of the instantaneous velocity at $\gamma = -30°$ under inflows: a) (i) and b) iii). The blue and black iso-surfaces of the flow volume force represent the blade and the turbulence grid, respectively. The tower and nacelle meshed surfaces appear in grey.

well reproduced.

The horizontal wake center deflection is depicted in Fig. 6 for $\gamma = -30°$ and $+30°$ and the three inflow conditions. The wake deflection quantification was made using an available power approach to replicate the experimental results [15] and to remove any method-dependant error. The computed wake center deflection is slightly larger than in the experiment, the difference of available data (larger in the LES) might induce such small variations. The TI-dependent wake deflection model of Bastankhah and Porté-Agel [14] is also presented for the two values of turbulent intensity. The model replicates properly the behavior of the LES until $x = 6D$. This model does not take into account the confinement of the wind tunnel and the wake has no constraint, drifting away from the turbine indefinitely. In contrast, the LES takes into account the confinement due to the wind tunnel walls and the wake center is redirected towards the center of the channel after $x = 6D$.

3.3. Performances and azimuthal loads

The final part of this paper studies the impact of the yaw angle on the turbine performances. The impact of the inflow on the time and azimuth averaged angle of attack α is low and for the sake brevity Fig. 7(a) presents the results only for the inflow iii). The most interesting aspect is the near hub variations of α due to azimuth for $\gamma = -30°$ and $+30°$. Indeed values fluctuate from $-5°$ up to $30°$ showing the potential appearance of dynamic stall in theses areas. Their respective positions are shifted from $180°$ between the two different yaw angles. On top of that, the negative angles of attack will directly impact the local force by giving a negative contribution to the global torque near the hub. The time averaged RMS of the azimuth average angle of attack are similar for inflow (ii) and (iii) but near zero for inflow i). Therefore, Fig. 7(b) presents these values only for the inflow iii). The angle of attack fluctuations are mainly present near the hub for the three yaw angle configurations, reaching oscillations up to $6°$. For $\gamma = -30°$ and $+30°$ the fluctuations arise where their mean value is maximal, triggering even more the potential
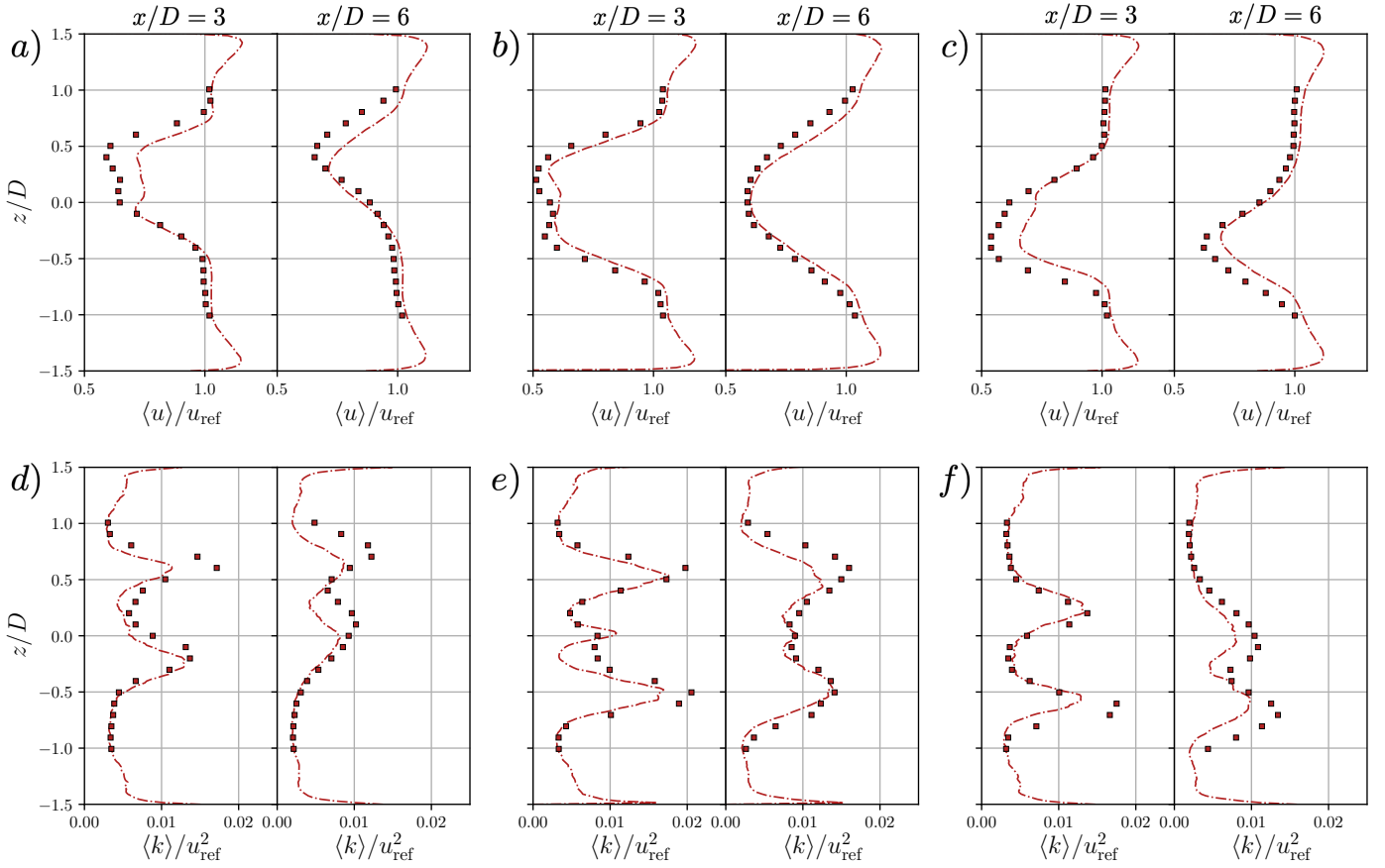
Figure 5. Horizontal profiles of the time-averaged streamwise velocity (a-c) and the turbulent kinetic energy (d-f) at $3D$ and $6D$ behind the turbine under inflow (iii) for the three yaw angles configuration: a,d) $\gamma = -30°$, b,e) $\gamma = 0°$ and c,f) $\gamma = +30°$. Experimental (■) and LES (‑·‑·) results are presented.

dynamic stall effect.

Table 2 presents the averaged power and thrust coefficients under inflow i), (ii) and (iii) for the different yaw angles, computed as

$$\langle C_P \rangle = \frac{8\langle P \rangle}{\pi \rho u_{\mathrm{ref}}^3 D^2}, \quad \langle C_T \rangle = \frac{8\langle T \rangle}{\pi \rho u_{\mathrm{ref}}^2 D^2}, \tag{1}$$

where P is the power, T the thrust force and ρ the fluid density. As expected by using standard ALM with no corrections (see subsection 2.1), the power production differs significantly regarding to the experimental data. Indeed, even if the profiles in the wake are in good accordance to the experiment, the retrieved power remains overestimated, up to 20% ($\gamma = +30°$, inflow i)). The thrust coefficient for the non yawed turbine case is slightly overestimated for all the inflows, while for the yawed cases, it is underestimated. Theses discrepancies between cases with or without yaw seem directly due to the error committed by not using a dynamic stall model in the near hub region for the yawed case.
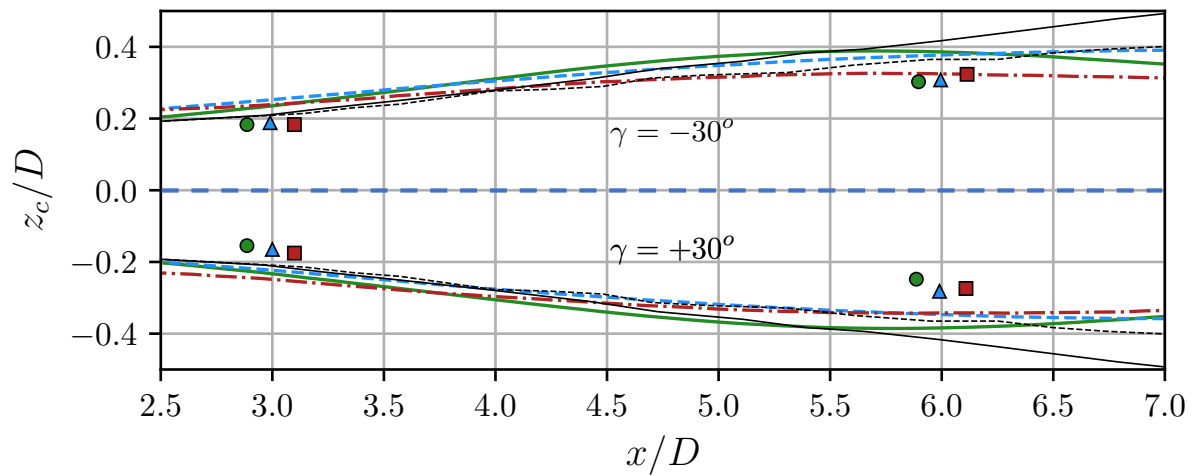
Figure 6. Calculated wake deflection z_c/D for $\gamma = -30°$ (top) and $+30°$ (bottom) under three different inflow conditions compared to experiment (at $3D$ and $6D$ only): (i) Experimental (●), LES (——); (ii) Experimental (▲), LES (- - -); (iii) Experimental (■), LES (-·-·). A comparison to the wake deflection model of Bastankhah and Porté-Agel [14] for TI_i (——) and TI_{ii} (- - -) is provided.
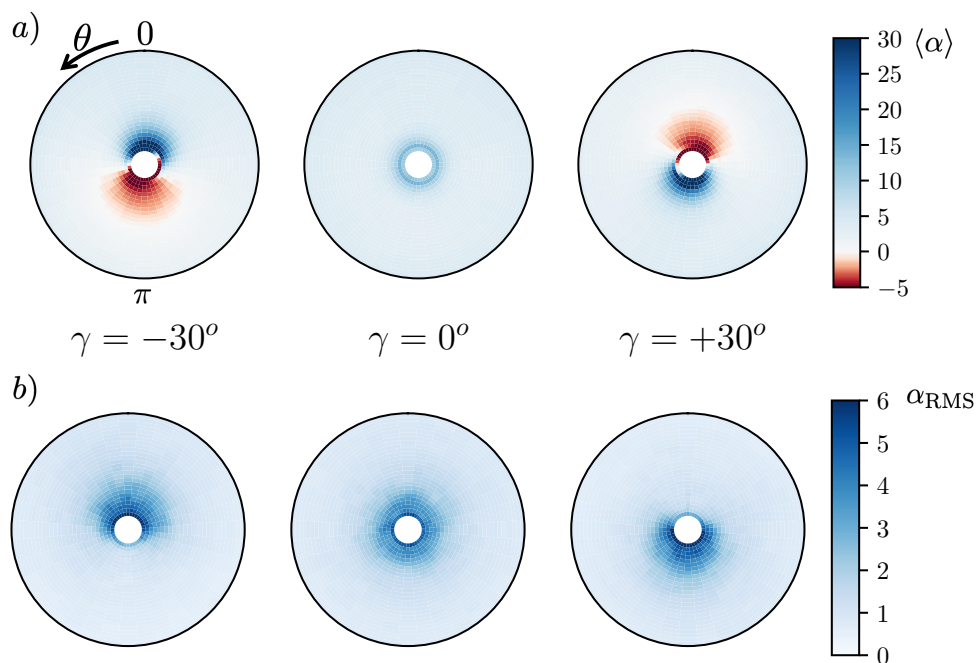
Figure 7. Radius and azimuth averaged temporal mean (a) and temporal RMS (b) of angle of attack for $\gamma = 30°$, $0°$ and $-30°$ under a non-uniform sheared inflow with a high turbulence level, inflow iii).

inflow	$\gamma = -30°$				$\gamma = 0°$				$\gamma = +30°$			
	$\langle C_P \rangle$	E_{C_P}	$\langle C_T \rangle$	E_{C_T}	$\langle C_P \rangle$	E_{C_P}	$\langle C_T \rangle$	E_{C_T}	$\langle C_P \rangle$	E_{C_P}	$\langle C_T \rangle$	E_{C_T}
(i)	0.382	+16%	0.64	-9%	0.553	+18%	0.91	+2%	0.387	+20%	0.65	-8%
(ii)	0.369	+11%	0.64	-9%	0.541	+15%	0.9	+3%	0.350	+8%	0.65	-7%
(iii)	0.371	+13%	0.62	-6%	0.544	+18%	0.89	+8%	0.368	+14%	0.63	-6%

Table 2. Time averaged power and thrust coefficients of the turbine (C_P and C_T) at the optimal operating point ($\lambda = 6$) for the three yaw angles and the three inflow conditions. The power E_{C_P} and thrust E_{C_T} errors are computed with respect to the experimental data from J. Bartl et al. [6].

4. Conclusions

The aim of this study was to evaluate the actuator line method in an LES framework for a yawed wind turbine with respect to an extensive experimental dataset. Different turbulent inflows were investigated and compared to a laminar inflow as well as the influence of yaw angle on the turbine property. For these cases the wake deviation, the azimuth discrepancies in the angle of attack and the turbine performances were discussed.

The paper first presents the capability to emulate a turbulent flow representative of the experimental wind tunnel grid. The uniform and non-uniform turbulent inflows were reproduced using dynamic actuator line method and have shown fairly good agreement to vertical velocity profiles and turbulent kinetic energy.

Regarding the wind turbine cases, the horizontal velocity and turbulent kinetic energy profiles reproduce the main features of the experimental data, yet slightly underestimated for the yawed cases. For the latter, the wake of the nacelle triggers the destabilization of the wake while for yaw angle $\gamma = 0°$ the nacelle-generated TKE is still observed $3D$ behind the turbine. The wake center is identified based on the minimum available power and compared to the wake center identified in experiments. The magnitude of the deflection is slightly overestimated compared to experiments. Comparison to wake deflection model shows a realignment of the wake due to the confinement induced by the wind tunnel walls. The azimuth and time averaged angle of attack points out the probability of dynamic stall near the hub of yawed turbines. The high level of turbulence present in the freestream contributes to it as well. The power coefficient differs significantly from the experimental measurements, up to $+20\%$ while the thrust is in better accordance with a deviation of up to 9%. The ability to retrieve the main features in the wake while mainly overestimating the loads has shown a missing piece lying in the generation of a yawed turbine wake.

This paper leaves the discussion of the use of ALM for a turbine under yaw conditions open, yet pointing out the necessity of specific corrections in such cases. Next studies should focus on the proper estimation of the loads and the comprehension of the aerodynamics of yawed rotors.

References

[1] Gebraad P M O, Teeuwisse F W, van Wingerden J W, Fleming P A, Ruben S D, Marden J R and Pao L Y 2016 *Wind Energy* **19** 95–114
[2] Breton S P, Sumner J, Sørensen J N, Hansen K S, Sarmast S and Ivanell S 2017 *Philosophical Transactions of the Royal Society A: Mathematical, Physical and Engineering Sciences* **375**
[3] Sørensen J and Shen W 2002 *J Fluids Eng* **124** 393–399

[4] Shen W Z, Zhu W J and Sørensen J N 2014 *Journal of Physics: Conference Series* **555**

[5] Meyer Forsting A R, Pirrung G R and Ramos-García N 2019 *Journal of Physics: Conference Series* **1256**

[6] Bartl J, Mühle F, Schottler J, Sætran L, Peinke J, Adaramola M and Hölling M 2018 *Wind Energ. Sci.* 329–343

[7] Satran L, Mühle F, Bartl J, Schottler J and Adaramola M S 2017

[8] Moureau V, Domingo P and Vervisch L 2011 *Comptes Rendus Mécanique* **339** 141–148

[9] Kraushaar M 2011 *Application of the compressible and low-Mach number approaches to Large-Eddy Simulation of turbulent flows in aero-engines* Ph.D. thesis INPT

[10] Benard P, Viré A, Moureau V, Lartigue G, Beaudet L, Deglaire P and Bricteux L 2018 *Computers & Fluids* **173** 133–139

[11] Shen W Z, Zhu W J and Yang H 2015 *Journal of Power and Energy Engineering* 7–13

[12] Duprat C, Balarac G, Métais O, Congedo P M and Brugière O 2011 *Physics of Fluids* **23** ISSN 10706631

[13] Houtin-Mongrolle F, Bricteux L, Bénard P, Lartigue G, Moureau V and Reveillon J 2020 Actuator line method applied to grid turbulence generation for large-eddy simulations Tech. rep. https://hal.archives-ouvertes.fr/hal-02496216

[14] Bastankhah M and Porté-Agel F 2016 *Journal of Fluid Mechanics* **806** 506–541

[15] Schottler J, Bartl J, Mühle F, Sætran L, Peinke J and Hölling M 2018 *Wind Energ. Sci.* 257–273